

Combined multiplanar optical coherence tomography and confocal scanning ophthalmoscopy

Adrian Gh. Podoleanu

George M. Dobre

Radu G. Cucu

University of Kent
School of Physical Sciences
Applied Optics Group
Canterbury, United Kingdom
E-mail: ap11@ukc.ac.uk

Richard Rosen

Patricia Garcia

Juan Nieto

Daniel Will

Ronald Gentile

Thomas Muldoon

Joseph Walsh

New York Eye and Ear Infirmary
Advanced Retinal Imaging Center
New York, New York

Lawrence A. Yannuzzi

Yale Fisher

Dennis Orlock

Lu Esther T. Mertz Retinal Research Center
New York, New York

Rishard Weitz

John A. Rogers

Shane Dunne

Aaron Boxer

Ophthalmic Technology Inc.
Toronto, Canada

Abstract. We demonstrate the clinical application of a multiplanar imaging system that simultaneously acquires *en face* (C-scan) optical coherence tomography (OCT) and the corresponding confocal ophthalmoscopic images, along with cross-sectional (B-scan) OCT at specifiable locations on the confocal image. The advantages of the simultaneous OCT and confocal acquisition as well as the challenges of interpreting the C-scan OCT images are discussed. Variations in tissue inclination with respect to the coherence wave surface alter the sampling of structures within the depth of the retina, producing novel slice orientations that are often challenging to interpret. We have evaluated for the first time the utility of C-scan OCT for a variety of pathologies, including melanocytoma, diabetic retinopathy, choroidal neovascular membrane, and macular pucker. Several remarkable new aspects of clinical anatomy were revealed using this new technique. The versatility of selective capture of C-scan OCT images and B-scan OCT images at precise points on the confocal image affords the clinician a more complete and interactive tool for 3-D imaging of retinal pathology. © 2004 Society of Photo-Optical Instrumentation Engineers. [DOI: 10.1117/1.1627778]

Keywords: optical coherence tomography; confocal; retinal imaging; depth-resolved imaging.

Paper 103012 received Apr. 4, 2003; revised manuscript received Jul. 30, 2003; accepted for publication Aug. 1, 2003.

1 Introduction

High-resolution imaging and tomographic assessments in the fundus of the eye have been greatly enhanced with the introduction of the confocal scanning laser ophthalmoscope (CSLO).¹ The influence of scattered light from outside the focal point within the target is suppressed by a pinhole in front of the photodetector and conjugate to the focal plane.^{2,3} The depth resolution of the CSLO technology is, however, limited to about 0.3 mm, owing to the cumulated effect of eye aberrations and the low numerical aperture of the eye.⁴

A method providing even higher resolution imaging of the retina is optical coherence tomography (OCT).⁵ In OCT, the depth is explored by scanning the optical path difference (OPD) between the object path and the reference path in an interferometer illuminated by a low coherence source. The maximum interference signal is obtained for OPD=0. For an OPD larger than the coherence length of the source used, the interference signal diminishes considerably, which determines the selection in depth of the OCT. Generally, using superluminescent diodes, an instrumental depth resolution better than 20 μm is achievable with OCT.

OCT has been largely used to create longitudinal images of the eye (analogous to ultrasound B-scan cross-sections), which are in-depth measurements through the retina.⁶ Practi-

cally, a B-scan image is constructed from many A-scans, which are reflectivity profiles versus depth. This technique of slicing the tissue was facilitated by a technical advantage; when the mirror is moved in the reference path, not only is the depth scanned, but a carrier signal is also generated.⁷ The carrier signal frequency is the Doppler shift produced by the longitudinal scanner itself (scanning along the axis of the system, Z, to explore the tissue in depth).

The ability to capturing similar depth information in slices of the tissue at orientations parallel to the retinal surface (*en face* images, or C-scans) is very attractive given the clinician's extensive experience with the ophthalmoscopic viewpoint and the growing popularity of the confocal scanning laser ophthalmoscopy technology.^{1–4,8}

In order to generate C-scan images at a fixed depth, a path imbalance modulator is needed to create a carrier for the image bandwidth. This will obviously require the introduction of a phase modulator in one of the arms of the interferometer, which would complicate the design and introduce dispersion.⁹ We have shown that the X or Y-scanning device itself introduces a path modulation that plays a role similar to that of the path modulation created by the longitudinal scanner in longi-

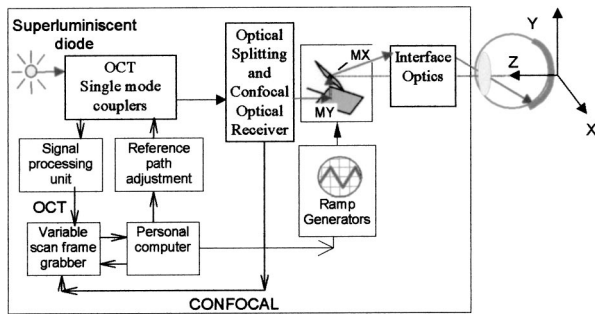


Fig. 1 General setup of the combined OCT and confocal system. MX, MY, galvanometer mirrors of the XY scanning head.

tudinal imaging OCT set ups. Theoretical analysis has shown that the OCT image production can be interpreted as interrogating the object with a specific sampling function. Depending on the position of the incident beam on the galvoscaner mirror and on the interface optics used, the sampling function could appear either as Newton rings¹⁰ or as a regular grid of lines.¹¹ The sampling function is in fact a fringe pattern in transversal section. Consequently, when the beam scans the target, the OCT signal is modulated by this fringe pattern. Since the pattern is not regular, the transversal resolution varies across the target and different frequencies result, in contrast to the OCT longitudinal imaging case where the carrier frequency is constant. However, we have shown¹² that for a sufficiently large image size, the errors introduced in the image by the variable sampling pattern can be neglected. For an image size larger than 1 mm, the external phase modulator has had little effect.

Here we demonstrate that images from eyes with pathologies can be generated using the same concept. An advanced prototype of a dual-channel OCT-confocal instrument¹³ is employed. The advantages of simultaneous OCT and confocal imaging are illustrated. Such a presentation of images addresses the incompatibility in correlating views of current CSLO and OCT systems. We discuss the superiority of *en face* OCT over the standard longitudinal OCT for transverse resolution, the synergy between the two channels, OCT and confocal, and the challenges of interpreting the C-scan OCT images. All these issues are discussed in relation to tilted and scattering features observed in cases such as melanocytoma, diabetic retinopathy, choroidal neovascular membrane, and macular pucker. We demonstrate the versatility of the dual-channel OCT-confocal instrument, which allows selective capture of different orientations of OCT images at precise points on the confocal image. This is facilitated by the high transverse resolution in the pairs of OCT and confocal images.

2 Instrument

The basic configuration of our system is shown in Fig. 1. The apparatus consists of an interferometer excited by a pigtailed superluminescent diode, central wavelength $\lambda = 0.82 \mu\text{m}$, bandwidth $\Delta\lambda = 20 \text{ nm}$, which sends $450 \mu\text{W}$ of power to the eye. The interferometer consists of fused directional single-mode couplers.¹² The sensing arm consists of a pair of X,Y galvanometer scanners to scan the ray angularly in rectangular

directions, followed by an interface optics to convey the scanned fan of rays through the eye pupil toward the retina. In the reference arm, a $1\text{-}\mu\text{m}$ resolution computer-controlled translation stage is employed to change the optical path and in this way, the depth at which the OCT signal is acquired.

A unique feature of our system is that it collects a corresponding confocal signal simultaneously with the OCT signal¹⁴ image. In the sensing arm of the OCT, a splitting device redirects a part of the light returned from the eye toward a photodetector behind a lens and a pinhole, used in a confocal receiver. The OCT and confocal signals carrying the information about the reflectivity of the target are sent to a dual-input, variable-scan frame grabber, which displays two images under computer control.

2.1 Regimes of Operation

The system can operate in different modes. In the B-scan mode, only one galvomirror of the galvanometer scanning pair is driven with a ramp at 700 Hz, and the translation stage is moved for the depth range required in 0.5 s. In this case, an OCT B-scan image is produced in either the x,z -plane or the y,z -plane.

In the C-scan mode, one galvoscaner is driven with a ramp at 700 Hz and the other with a ramp at 2 Hz. In this way, C-scan images in the x,y -plane are generated in both channels. The depth at which the OCT C-scan image is collected is changed by moving the translation stage in the reference arm of the interferometer in Fig. 1.

The frame grabber has two inputs, each equipped with an 8 bit analog-to-digital (A/D) converter, and displays a pair of two images, each with 480 lateral and 350 vertical pixels irrespective of the regime of operation, B-scan or C-scan. The images are pixel-to-pixel correspondent and such pixels are constructed simultaneously in the two images, first along lines in the rasters and then from the end of the line to the beginning of the next consecutive line. Therefore the two images are acquired and constructed simultaneously.

In the B-scan regime, the frame grabber operates under the control of the generator driving the galvanometer scanner and the translation stage. Each line in both images is triggered by the generator driving the galvanometer scanner (700 Hz), while the generation of the frame of the pair of images is triggered by the translation stage (every 0.5 s). The horizontal size of the OCT is determined by the magnitude of the signal applied to the galvanometer scanner, while the vertical size corresponds to depth. The image in the confocal channel consists of repeated distributions of the intensity of the signal collected. The horizontal size is the same as that of the OCT image, while the vertical size represents time.

In the C-scan regime, the frame grabber operates under the control of the generators driving the two galvanometer scanners. Each line in both images is triggered by the faster generator (700 Hz), while the generation of the frame of the pair of images is triggered by the slower generator (2 Hz). The horizontal size of the OCT and confocal images is determined by the magnitude of the signal applied to the fast galvanometer scanner, while the vertical size in both images is determined by the magnitude of the signal applied to the slow galvanometer scanner. Operating at two frames a second, this means that the two images are constructed from the top left

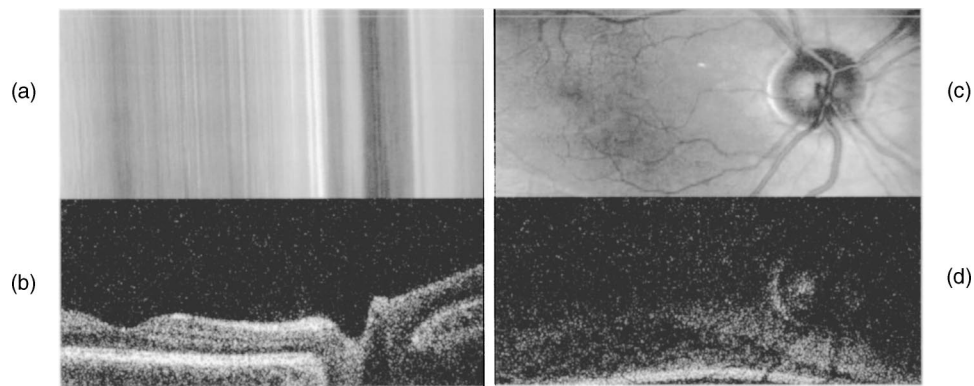


Fig. 2 Images of a normal eye generated with the stand-alone OCT-confocal system showing the fovea and the optic nerve. Transverse pixel size, $<20 \mu\text{m}$; depth pixel size, $<13 \mu\text{m}$ in tissue. Lateral size in all images, 35 deg (horizontal). (a) and (b) B-scan mode: Only the horizontal transverse scanner is driven; (a) is a repetition of linear *en face* scan profiles in time, at different moments while the depth in the range of 1 mm in the OCT channel is changed to produce the longitudinal OCT in (b). The 1-mm depth is along the vertical axis in (b) only, measured in air. The image features details of the optic nerve, foveal depression, and inner retinal layers, such as the retinal nerve fiber layer and the retinal pigment epithelium. (c) and (d) C-scan mode: Both the horizontal and vertical transverse scanners are driven; (c) is the confocal image in the pair and (d) is a deep C-scan OCT at the level of the choroid, demonstrating its characteristic vascular lobules. Vertical size, 15 deg.

corner pixel, at coordinates (1,1), then line by line till the end of a frame period of 0.5 s, when the last pixel (480, 350) in the bottom right corner of each image is displayed.

In comparison with previous reports,¹⁴ we have improved the interface optics to expand the field of images collected from the retina and include both the fovea and the optic nerve in a single frame. Such images from the right eye of one of the authors (AP), illustrating the two regimes of operation are shown in Fig. 2. Each pair of images was obtained in 0.5 s. The pair of images in Figs. 2(a) and 2(b) was obtained in the B-scan regime, while the pair of images in Figs. 2(c) and 2(d) was obtained in the C-scan regime. The images in Figs. 2(a) and 2(c) are delivered by the confocal channel while the images in Figs. 2(b) and 2(d) are delivered by the OCT channel. The signal in the confocal channel is determined by the reflectivity of the target, while in the OCT channel it is determined by the square root of the same reflectivity. In other words, a strong change in the index of refraction from a scattering point to the surrounding medium is indicated by a signal of high intensity in both channels.

Achieving an image size of a 35-deg angle was made possible by further refinement of the scanning elements and processing electronics to cope with the subsequent increase in the bandwidth. The image bandwidth is proportional to the scanning rate and image size, and in this case components up to 300 kHz are generated. We have, however, slightly compromised the transverse size resolution and reduced the electronic bandwidth to 200 kHz to achieve a signal-to-noise ratio before the frame grabber of more than 40 dB, a value close to the dynamic range of the 8-bit A/D converter used in the frame grabber. In evaluating the signal-to-noise ratio, we used the signal reflected from the retinal pigment epithelium (RPE).

However, in interpreting the pathology cases that follow, we present smaller size images (15 and 20 deg) for better display of tiny features. When collecting smaller sized images, we maintained the same electronic bandwidth of 200 kHz and the same frame rate, 2 Hz.

In the images presented in this paper, no other phase modulation was employed apart from that introduced by the X-galvanometer scanner. We previously demonstrated the role played by the image size¹² in balancing the effects of an external phase modulator and of the modulation produced by the transversal scanner. For instance, when the image size was six times smaller than that of the images in Fig. 2, it was advantageous to employ a phase modulator working at $f = 30 \text{ kHz}$.

2.2 Resolutions

Because the focus is not changed when the path imbalance in the OCT is altered, the confocal image does not change with depth z . Therefore all the lines in Fig. 2(a) are essentially the same; each line is the linear variation of the intensity received along the X-axis at different moments of time during the frame time interval. Similarly, the image in Fig. 2(c), which is the (x,y) map of the intensity, is the same in all the pairs of images collected at different positions of the translation stage.

Using a plane mirror in the object arm, the FWHM of the depth sampling interval in both channels was determined. To determine the depth resolution of the OCT channel, a very small amplitude was applied to the galvanometer scanner operating at 700 Hz to create a path modulation larger than $\lambda/2$, while no voltage was applied to the other galvanometer scanner. Using the translation stage, shifted either side of the maximum of interference until the intensity fell to half, a depth resolution in air of $18 \mu\text{m}$ was obtained for the OCT channel. The depth sampling interval in tissue can be obtained by dividing this value by the index of refraction (this varies, depending on the tissue; however, an average value of 1.36 can be used¹⁵), leading to about $13 \mu\text{m}$. Obviously, this is the ultimate resolution achievable for stationary tissue only. The interpretation of the images in Figs. 2(b) and 2(d) should consider that the two frame/s rate is relatively low compared with the equivalent axial speed resulting from microsaccades, blood pulsations, and head movements. Therefore the images will not be artifact free in this respect.

To determine the FWHM of the depth profile of the confocal channel, the voltages on the galvanometer scanners were brought to zero and the mirror moved through focus until half of the value of the signal obtained in the focus was obtained, which led to an FWHM of 5.3 mm in air.¹⁴ This value was determined by the pinhole size (30 μm) and the focusing lens (1.5-cm focal length microscope objective) in the confocal receiver, which have been adjusted as a tradeoff between the image strength and elimination of stray reflections from the interface optics and the cornea. The choice of pinhole size is related to the beamsplitter ratio;¹⁴ the smaller the percentage diverted from the backscattered signal to the confocal receiver, the larger the pinhole size should be. Since the depth-resolved information is provided by the OCT images, the depth resolution of the confocal channel is less important as long as the stray reflections are sufficiently attenuated. The role of the confocal channel is to provide lateral and contextual information, owing to its better transverse resolution, and in this way the two imaging systems complement each other.

Because the confocal receiver is far from ideal,¹⁴ the transverse resolution in the confocal channel is practically that of a conventional microscope. The beam diameter output from the instrument to the eye is 3 mm. This should determine a lateral resolution better than 5 μm . It is known, however, that owing to eye aberrations¹⁶ and scattering, an ideal confocal channel for a 3-mm aperture is not expected to achieve better than a 10 to 15- μm transverse resolution from the back of the eye.¹⁷

Owing to the way the carrier is created in the OCT channel¹⁰⁻¹² and the speckle effects, it was expected that the transverse resolution in the OCT channel would be worse than that of the confocal channel. However, using a plane target of holes and lines at the back of a lens of 2 cm focal length, the transverse resolution was found to be better than 20 μm in both channels.

3 Dual Imaging Technology

3.1 *En Face* Scanning Allows High Transversal Resolution

As a result of transverse scanning, the B-scan OCT image in our system is continuous along the line in the raster, as opposed to B-scan OCT images generated using fast axial scanning, where the lateral scanning is discrete. This improves the quality of the images, as demonstrated later. Although our OCT system has only a 12- μm depth resolution in tissue, the B-scan image in Fig. 2(b) looks similar to the B-scan image generated by the group at Massachusetts Institute of Technology¹⁸ using longitudinal OCT and a much higher depth resolution, of 3 μm in tissue. Any connectivity or association between scatterers in the transverse section is better conserved when performing *en face* scanning. This ultimately allows visualization of small protuberances on the retina, as demonstrated in this paper with several cases of pathology.

3.2 Synergy between the Channels

In terms of data acquisition, the confocal image adds further versatility. The design ensures a strict pixel-to-pixel correspondence between the two C-scan images (OCT and confocal). This helps in two respects: for small movements, the confocal image can be used to track the eye movements between frames and for subsequent transversal alignment of the

OCT image stacks; for large movements and blinks, the confocal image gives a clear indication of the OCT frames that need to be eliminated from the collected stack. As a reference for the aligning procedure, the first artifact-free confocal image in the set is used. For example in Fig. 2(a), movements of the eye are indicated by lateral shifts of the confocal traces. Each horizontal line in the confocal image corresponds to a depth position. The relative eye movement, proven by the slight deviation of shadows to the right, can easily be utilized to correct the lateral shift of the lines in the B-scan OCT image in Fig. 2(b).

3.3 3-D Imaging

3-D imaging of the retina is already common with CSLO technology.¹⁹ The use of *en face* sections collected from different depths²⁰ to construct a 3-D profile of the retina is already accepted and understood by ophthalmologists. The stand-alone OCT-confocal system can proceed in the same way, however, with *en face* slices as thin as allowed by the OCT technology. To collect the reflectivity distribution from the volume of the retina, the stand-alone OCT-confocal system is operated in the C-scan mode, collecting *en face* images at different depths. Ideally, the depth interval between successive frames should be much smaller than the system resolution in depth, and the depth change should be applied only after the entire C-scan image is collected. However, in practice, to speed up the acquisition, the translation stage is moved continuously and the depth interval is set slightly larger than the depth resolution.²¹ For instance, using 20 μm between frames, 60 frames of image pairs from a volume in depth of 1.2 mm in air (which is sufficient to cover the volume of the retina around the optic nerve) can be acquired in 30 s when operating at a 2-Hz frame rate. After acquisition, the images can be aligned transversally using the first confocal image (or the first consistent confocal image) and then the stack of OCT images or the stack of the pairs of OCT and confocal images can be used to construct a 3-D profile of the volume of the retina.^{21,22} It is much easier to align the pairs of images in this way than aligning C-scan OCT images that have different features for different depths.

3.4 Topography

The topography of the fundus is difficult to obtain using A-scan images. A procedure using A-scans is cumbersome because it requires interpolation in the *en face* plane.²³ Owing to a wide variety of features being available to use for interpolation, with many of these being of high contrast, it is likely to be more accurate to construct the topography using *en face* scanning. The topography in itself outputs an *en face* image, which makes the *en face* OCT more suited for signal processing. Such a procedure using collected *en face* images was described in a previous report.²⁴ Based on *en face* OCT, obtaining a topography should be similar to the method using a CSLO.²⁵

3.5 New Challenge

New imaging technology not only brings new information to the clinician, but with it the requirement of interpretation. *En face* OCT is no exception in this respect. The higher the depth resolution of the OCT system, the more fragmented the *en*

face OCT image looks.²⁶ Since the imaging proceeds at a few frames a second, the inherent eye movements may result in significant changes in the size of fragments sampled from the tissue. The fragmentation is especially visible when imaging very inclined tissue. The *en face* OCT image in Fig. 2(d) shows the challenges in interpreting and using these images. First, the *en face* OCT image looks fragmented, and on its own, such an image cannot be interpreted. Second, variations in tissue inclination with respect to the coherence wave surface alter the sampling of structures within the depth of the retina,²⁷ producing novel slice orientations that are often challenging to interpret.

The bright patches in the OCT image represent the intersection of the surface of the optical path difference (OPD) = 0 with the tissue. Owing to the particular way the retina is scanned, with the fan of rays converging on the eye's pupil, the surface of OPD=0 is an arc circle with the center in the eye's pupil. When we explore the depth, we change the radius of the arc. If the arc has a small radius, it may just only intersect the top of the optic nerve, with the rest of the arc in the aqueous. The radius of the arc is changed by changing the length of one of the arms of the interferometer in the OCT channel to explore the retina up to the RPE and choroid. The orientation of the retina tissue at the back of the eye is not planar, and this complicates the interpretation of the image even further.

Another issue is that despite scanning images *en face*, the images may display the structure in depth, as in any longitudinal OCT image. These two effects—fragmentation and depth structure—displayed in the C-scan images are present in a CSLO with high depth resolution as well; however they occur at a scale where they are regularly discarded. In a CSLO, the images do not look fragmented and the depth structure is barely visible, owing to the coarse depth resolution (0.3 mm), which is comparable to the retina's thickness. Going in and out of focus results in a smooth transition from dark to bright of areas in the image. Both problems mentioned earlier are brought about by the high depth resolution of OCT. We address the fragmentation problem by providing the confocal image, which guides the user, and by collecting many *en face* images at different depths and subsequently building the 3-D profile. The other problem—that the *en face* image may also display the depth structure—requires further development of the interpretation process.

4 Eyes with Pathology

The utility of the dual display in helping the clinician to understand the morphology below the surface as well as the interpretation challenges raised by this new imaging technology are best revealed by examining sample image sets. All images were collected using a sturdy, specially designed chin rest, but no bite bars, as is common in ophthalmology practice when seeing patients. Therefore some movements effects in the images are visible.

The images in Fig. 3 display a case of melanocytoma.²⁸ A pair of C-scan OCT and confocal images is shown in Figs. 3(a) and 3(b). Two other C-scan OCT images from different depths are shown in Figs. 3(c) and 3(d) (the paired confocal image for each is the same as that in Fig. 3(a); therefore the confocal images are not repeated). The C-scan images in Figs.

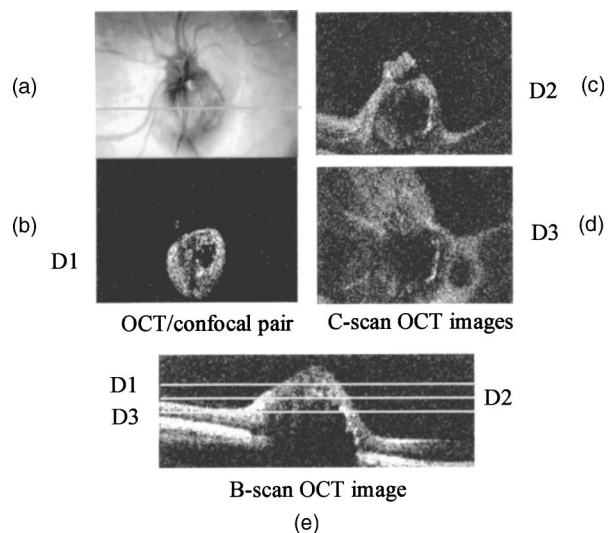


Fig. 3 Melanocytoma. The lines D1, D2, and D3 in the B-scan OCT image (e) show the depths at which the C-scan OCT images (b), (c), and (d) were collected. The B-scan in (e) has been sampled in depth along the line shown in the confocal image in (a). Angular size, 15 × 15 deg. Depth in the B-scan image, 2 mm measured in air.

3(b) 3(c), and 3(d) are collected from depths D1, D2, and D3 as indicated in the B-scan OCT image in Fig. 3(e), respectively, while the B-scan image in Fig. 3(e) has been sampled in depth along the line shown in the confocal image in Fig. 3(a). By collecting a stack of OCT-confocal images, the volume of the retinal elevation could be evaluated.

The line D1 in Fig. 3(e) shows the limitation of imaging small-sized features on the retina using the B-scan OCT only.

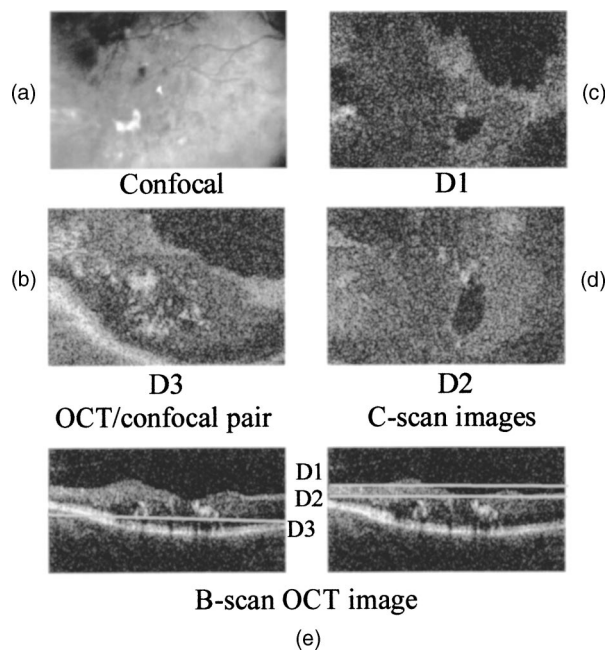


Fig. 4 Diabetic retinopathy. The lines D-1, D-2, and D-3 in the B-scan OCT image (e) show the depths at which the C-scan OCT images (b) to (d) were collected. Angular size, 15 × 15 deg. Depth in the B-scan image, 2 mm measured in air.

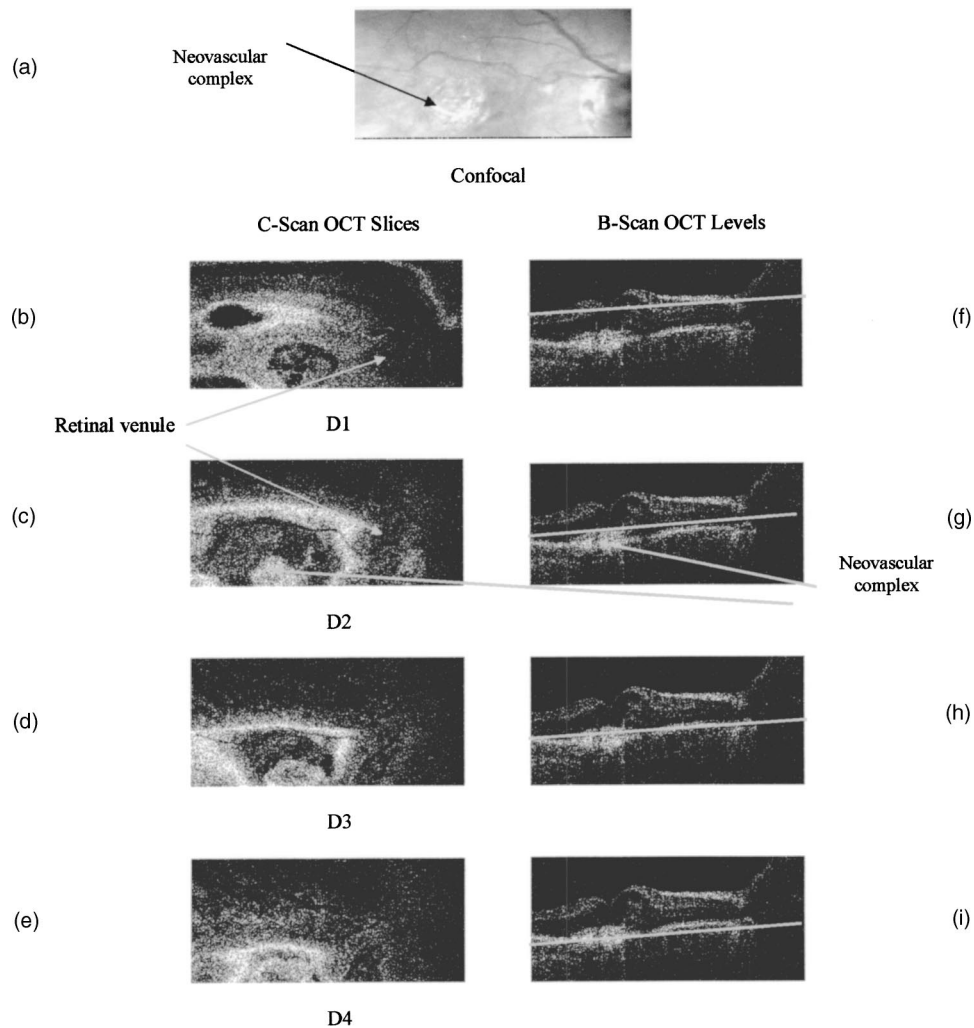


Fig. 5 Choroidal neovascular membrane with overlying cystoid macular edema in a patient with wet age-related macular degeneration. The gray lines on the paired B-scan OCT images (f) to (i) indicate the level at which the 20×20-deg C-scans (b) to (e) were acquired. Depth in the B-scan images, 2 mm measured in air.

Serial samples at sequential transverse locations would be required to create the 3-D profile. Targeting such small deformations requires good transverse resolution, which is made possible in this instrument by the confocal channel. Accurate volume assessment requires collection of a serial stack of C-scans at progressive depths. While the current instrument is equipped with such a feature, we had variable success using it in eyes with a pathology because of their limited ability to maintain consistent fixation. We have found another feature of the system more useful; this allows an easy switch between the two modes, B-scan and C-scan. Successive C-scan cuts with checks in the transverse section using the B-scan images allowed us to obtain a 3-D picture of the lesion despite the eye movements.

Interpretation of these images requires some careful thought. Owing to the inclination of the walls of the thickened retina, the C-scan images often display depth structures, as seen in the OCT images in Figs. 3(b), 3(c), and 3(d). As such, the C-scan OCT images alone may lead to a wrong interpretation. Comparing them with the B-scan image at the Fig. 3(e) is helpful in establishing the orientation and the depths of

features depicted in individual scans. The images in Fig. 3 show the two challenging features of the high-resolution C-scan imaging: patchy fragmented planes and display of depth structure for the tilted parts of the tissue. The elongated parts visible in the B-scan OCT images in Fig. 3(e) show up as holes of different intensities in the C-scan images, which indicate different structures in depth owing to the discontinuity of optical parameters, such as the index of refraction and backscattering coefficient. When we follow the cuts along the straight lines indicated, we can infer the intensity level in the corresponding part of the C-scan OCT image in Figs. 3(b), 3(c), and 3(d). Evaluating how the radius of the dark circles in Figs. 3(b), 3(c), and 3(d) varies with depth, the volume of the lesion can be easily inferred.

Similar challenges are presented in the interpretation of the images in Fig. 4, a case of diabetic retinopathy.²⁹ The confocal image and three C-scan OCT images [Figs. 4(b) to 4(d)] are shown. For ease in interpretation, the B-scan OCT [Fig. 4(e)] is duplicated underneath each column of images. In Fig. 4(b) the C-scan OCT image at depth D3 samples the RPE near the left edge of the scan, owing to the curvature of the retina. At

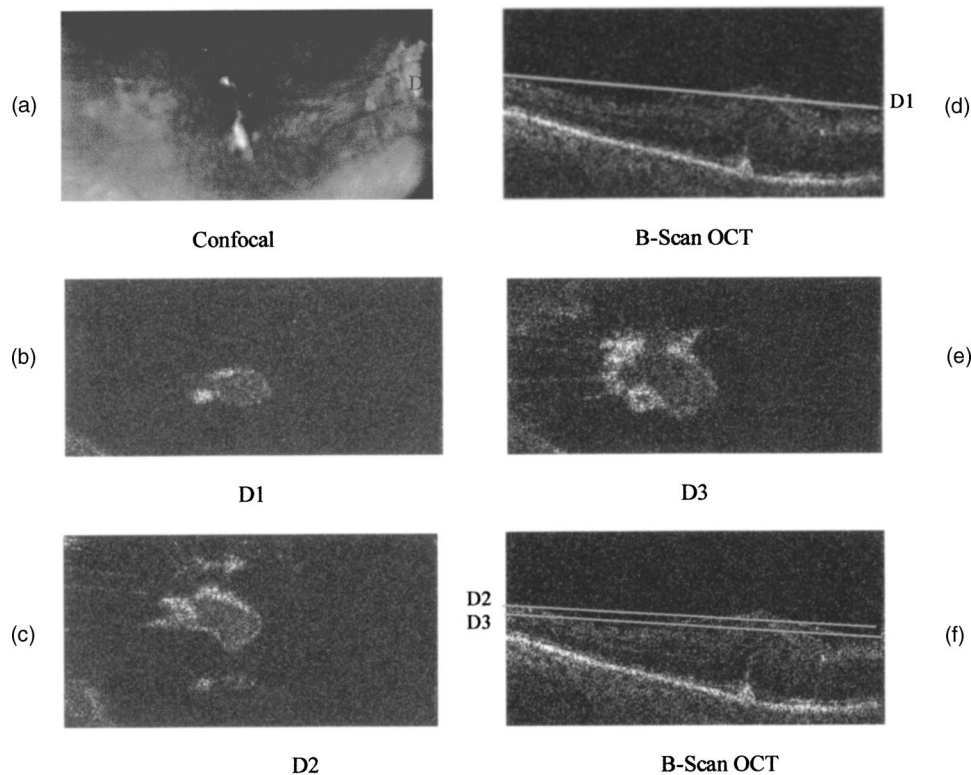


Fig. 6 Macular pucker due to epiretinal membrane. The gray lines on the B-scan OCT images (d) and (f) indicate the level of the accompanying C-scan OCT slices (b), (c), and (e). The thickness and expanse of the membrane can be calculated from the thickness of intervening slices. Depth in the B-scan images, 2 mm measured in air.

this level, near the base of the foveal depression, the edema residues are spread diffusely. In levels D1 and D2, the dark holes are created by the slices through the foveal cone at different levels. The white edema residues are seen at the edge of the cone. The confocal image Fig. 4(a) displays the clinical appearance of the surface, which reveals only limited details of the underlying pathological features.

Figure 5 demonstrates further how C-scan OCT images can enhance the understanding of anatomical relationships among different aspects of pathological processes that affect complex retinal structure. The images presented are from a case of exudative age-related macular degeneration with a choroidal neovascular membrane³⁰ and overlying cystoid macular edema. While these two aspects of the lesion can be identified in the cross-sectional aspect of the B-scan OCT [Figs. 5(f) to 5(i)], separate C-scan slices [Figs. 5(b) to 5(e)] reveal a more complete picture at the various interfaces of the components. The transverse direction of scanning is particularly effective at differentiating structure oriented horizontally.

The confocal view of the retina seen in Fig. 5(a) shows a diffusely increased reflex over a thickened central macula. The pairs below Fig. 5(a) demonstrate progressively deeper C-scan slices [Figs. 5(b) to 5(e)] and paired B-scans [Figs. 5(f) to 5(i)] marked with lines indicating their depth. Slice D1 is taken though the inner retina and cuts through multiple perifoveal cysts. The slice can be localized to the nerve fiber layer since it is at the same level of the retinal venule, which appears bright in the slice.

Slice D2 cuts through the lower aspect of the cystic area, which is seen surrounding the upper part of the neovascular complex. In this slice the venule outline is dark since it is a shadow cast from the layer above. Slice D3 cuts through the center of the neovascular complex, which appears highly reflective in the image. There is a dark crescent within the bright ring that is due to a slight tilt of the retina in relation to the plane of the scan. Slice D4 shows the neovascular complex as a bright mass surrounded by darker choroidal vessels.

Another important example of a pathology that demonstrates the clinical utility of the C-scan approach over the simple planar imaging of B-scan OCT is seen in the case of a macular pucker³¹ (Fig. 6). The confocal image in Fig. 6(a) shows the dragging of retinal blood vessels and loss of clarity characteristic of the epiretinal membranes that distort the macula. B-scan OCT images have become standard clinical tools for displaying the bunching up of the vitreoretinal interface under the cellophane-thin but contracting blanketing membrane. The difficulty clinicians often encounter in approaching these membranes surgically is in defining their lateral extent in order to plan minimally damaging peeling. The C-scan slices in Figs. 6(b), (c), and (e) reveal the tentaclelike extensions of the overlying tissue and help define the thickness and spread of the irregularly shaped growth.

5 Conclusions

Multiplanar OCT-confocal ophthalmoscopy combines two technologies, adding a new dimension to C-scan OCT, and

addresses the incompatibility in correlating views of current CSLO and OCT systems. The pixel-to-pixel correspondence inherent in the design of this system holds the promise of more complete and accurate volumetric and topographic analyses of the optic nerve and macula than is currently possible. The high transverse resolution in the pairs of OCT and confocal images allows a precise collection of B-scan images from any desired location on the confocal image.

The expanded field of images captured by this system is a significant improvement over smaller previously reported images of healthy eyes^{12,14,18} and enhances its clinical utility. The system offers: (1) versatility, being capable of displaying both C-scan and B-scan OCT images; (2) image alignment and orientation of retinal surface landmarks using the confocal image; and (3) correction for transverse movements in the B-scan OCT images using the confocal image.

Currently, C-scan OCT images are more challenging to interpret than B-scan OCT images and are more susceptible to eye movements. Additional efforts are under way to make full use of a successive switch between the B-scan and C-scan modes as well to construct 3-D volumes using stacks of C-scan images collected at different depths. Utilizing the expertise of clinicians in interpreting OCT and CSLO images from the current generation of commercially available systems, we believe that this new fusion of imaging technologies will yield substantial new insights into the intricate anatomy of retinal disease.

Acknowledgments

The authors are grateful to the Engineering and Physical Sciences Research Council of the United Kingdom, the New York Eye and Ear Infirmary Ophthalmology Research Fund, the University of Kent, and Superlum Moscow.

References

- R. H. Webb, G. W. Hughes, and F. C. Delori, "Confocal scanning laser ophthalmoscope," *Appl. Opt.* **26**, 1492–1499 (1987).
- A. E. Elsner, S. A. Burns, J. J. Weiter, and F. C. Delori, "Infrared imaging of sub-retinal structures in the human ocular fundus," *Vision Res.* **36**, 191–205 (1996).
- W. H. Woon, F. W. Fitzke, A. C. Bird, and J. Marshall, "Confocal imaging of the fundus using a scanning laser ophthalmoscope," *Br. J. Ophthalmol.* **76**, 470–474 (1992).
- D. U. Bartsch and W. R. Freeman, "Axial intensity distribution analysis of the human retina with a confocal scanning laser tomograph," *Exp. Eye Res.* **58**, 161–173 (1994).
- D. Huang, E. A. Swanson, C. P. Lin, J. S. Schuman, W. G. Stinson, W. Chang, M. R. Hee, T. Flotte, K. Gregory, C. A. Puliafito, and J. G. Fujimoto, "Optical coherence tomography," *Science* **254**, 1178–1181 (1991).
- D. S. Chauhan and J. Marshall, "The interpretation of optical coherence tomography images of the retina," *Invest. Ophthalmol.* **40**, 2332–2342 (1999).
- J. A. Izaat, M. R. Hee, G. M. Owen, E. A. Swanson, and J. G. Fujimoto, "Optical coherence microscopy in scattering media," *Opt. Lett.* **19**, 590–592 (1994).
- J. P. Kelly, A. H. Weiss, Q. Zhou, S. Schmode, and A. W. Dreher, "Imaging a child's fundus without dilation using a handheld confocal scanning laser ophthalmoscope," *Arch. Ophthalmol. (Chicago)* **121**(3), 391–396 (2003).
- C. K. Hitzengerger, A. Baumgartner, and A. F. Fercher, "Dispersion-induced multiple signal peak splitting in partial coherence interferometry," *Opt. Commun.* **154**, 179–185 (1998).
- A. Gh. Podoleanu, G. M. Dobre, D. J. Webb, and D. A. Jackson, "Coherence imaging by use of a Newton rings sampling function," *Opt. Lett.* **21**, 1789–1791 (1996).
- A. Gh. Podoleanu, G. M. Dobre, and D. A. Jackson, "En face coherence imaging using galvanometer scanner modulation," *Opt. Lett.* **23**, 147–149 (1998).
- A. Gh. Podoleanu, M. Seeger, G. M. Dobre, D. J. Webb, D. A. Jackson, and F. Fitzke, "Transversal and longitudinal images from the retina of the living eye using low coherence reflectometry," *J. Biomed. Opt.* **3**, 12–20 (1998).
- A. Gh. Podoleanu and D. A. Jackson, "Combined optical coherence tomograph and scanning laser ophthalmoscope," *Electron. Lett.* **34**(11), 1088–1090 (1998).
- A. Gh. Podoleanu and D. A. Jackson, "Noise analysis of a combined optical coherence tomography and confocal scanning ophthalmoscope," *Appl. Opt.* **38**, 2116–2127 (1999).
- C. K. Hitzengerger, "Optical measurement of the axial eye length by laser Doppler interferometry," *Invest. Ophthalmol. Visual Sci.* **32**, 616–624 (1991).
- A. Roorda, F. Romero-Borja, W. J. Donnelly III, H. Queener, and T. J. Hebert, "Adaptive optics scanning laser ophthalmoscopy," *Optics Express* **10**(9), 405–412 (2002).
- D. T. Miller, D. R. Williams, G. M. Morris, and J. Liang, "Images of cone photoreceptors in the living human eye," *Vision Res.* **35**(8), 1067–1079 (1995).
- W. Drexler, U. Morgner, R. K. Ghanta, F. X. Kartner, J. S. Schuman, and J. G. Fujimoto, "Ultrahigh-resolution ophthalmic optical coherence tomography," *Nat. Med. (N.Y.)* **7**(4), 502–507 (2001).
- D. U. Bartsch, M. Intaglietta, J. F. Bille, A. W. Dreher, M. Gharib, and W. R. Freeman, "Confocal laser tomographic analysis of the retina in eyes with macular hole formation and other focal macular diseases," *Am. J. Ophthalmol.* **108**(3), 277–287 (1989).
- F. E. Kruse, R. O. W. Burk, H. E. Volcker, G. Zinser, and U. Harbarth, "Reproducibility of topographic measurements of the optic nerve head with laser tomographic scanning," *Ophthalmology* **96**, 1320 (1989).
- A. Gh. Podoleanu, J. A. Rogers, D. A. Jackson, and S. Dunne, "Three dimensional OCT images from retina and skin," *Opt. Express* **7**(9), 292–298 (2000), <http://www.opticsexpress.org/abstract.cfm?URI=OPEX-7-9-292>.
- http://www.ukc.ac.uk/physical-sciences/aog/Low_Cohe/
- M. R. Hee, C. A. Puliafito, J. S. Duker, E. Reichel, J. G. Coker, J. R. Wilkins, J. S. Schuman, E. A. Swanson, and J. G. Fujimoto, "Topography of diabetic macular edema with optical coherence tomography," *Ophthalmology* **105**(2), 360–370 (1998).
- J. A. Rogers, A. Gh. Podoleanu, G. M. Dobre, D. A. Jackson, and F. W. Fitzke, "Topography and volume measurements of the optic nerve using en face optical coherence tomography," *Opt. Express* **9**(10), 476–545 (2001), <http://www.opticsexpress.org/abstract.cfm?URI=OPEX-9-10-533>.
- A. W. Dreher, P. C. Tso, and R. N. Weinreb, "Reproducibility of topographic measurements of the normal and glaucomatous optic nerve head with the laser tomographic scanner," *Am. J. Ophthalmol.* **111**, 221–229 (1994).
- A. Gh. Podoleanu, J. A. Rogers, and D. A. Jackson, "OCT en face images from the retina with adjustable depth resolution in real time," *IEEE J. Sel. Top. Quantum Electron.* **5**(4), 1176–1184 (1999).
- M. Ohmi, K. Yoden, and M. Haruna, "Optical reflection tomography along the geometrical thickness," *Proc. SPIE* **4251**, 76–80 (2001).
- B. A. Lafaut, H. Mietz, M. Ortmann, and K. U. Bartz-Schmidt, "Melanocytoma of the choroid: angiographic and histopathologic findings," *Ophthalmic Surg. Lasers* **33**(2), 158–162 (2002).
- W. N. Wykes, A. A. E. Pyott, and V. G. M. Ferguson, "Detection of diabetic-retinopathy by scanning laser ophthalmoscopy," *Eye* **8**, 437–439 (1994).
- T. Hashimoto and T. Harada, "Confocal scanning laser microscopic findings of excised choroidal neovascular membranes of age-related macular degeneration and their comparison with the clinical features," *Jpn. J. Ophthalmol.* **43**(5), 375–385 (1999).
- E. M. Messmer, H. P. Heidenkummer, and A. Kampik, "Ultrastructure of epiretinal membranes associated with macular holes," *Graefes Arch. Clin. Exp. Ophthalmol.* **236**(4), 248–254 (1998).